Consideration of the mechanisms for tidal bore formation in an idealized planform geometry

Daniele P. Viero[1], **Andrea Defina**[1,2]

[1]Department ICEA, University of Padova, Via Loredan 20, 35131 Padova, Italy.
[2]Intl. Center of Tidal Hidro- and Morphodynamics, University of Padova, Italy.

Key Points:

- The formation of tidal bores is investigated numerically within a schematic framework.
- A phenomenological analysis revealed the occurrence of nontrivial distinctive behaviors.
- The proposed criterion to predict tidal bore occurrence performs favorably also for real estuaries.

Corresponding author: D. P. Viero, `daniele.viero@unipd.it`

Abstract

A tidal bore is a positive wave traveling upstream along the estuary of a river, generated by a relatively rapid rise of the tide, often enhanced by the funneling shape of the estuary. The swell produced by the tide grows and its front steepens as the flooding tide advances inland, promoting the formation of a sharp front wave, that is, the tidal bore. Because of the many mechanisms and conditions involved in the process, it is difficult to formulate an effective criterion to predict the bore formation. In this preliminary analysis, aimed at bringing out the main processes and parameters that control tidal bore formation, the degrees of freedom of the problem are largely reduced by considering a rectangular channel of constant width with uniform flow, forced downstream by rising the water level at a constant rate. The framework used in this study is extremely simple, yet the problem is still complex and the solution is far from being trivial. From the results of numerical simulations, three distinctive behaviors emerged related to conditions in which a tidal bore forms, a tidal bore does not form, and a weak bore forms; the latter has a weakly steep front and after the bore formed it rapidly vanishes. Based on these behaviors, some criteria to predict the bore formation are proposed and discussed. The more effective criterion, suitably rearranged, is checked against data from real estuaries and the predictions are found to compare favorably with the available data.

1 Introduction

A tidal bore is a positive wave traveling upstream along the estuary of a river, generated by a relatively rapid rise of the tide, often enhanced by the funneling shape of the estuary. The swell produced by the tide grows and its front steepens as the flooding tide advances inland promoting the formation of a sharp front wave, that is, the tidal bore. Freshwater river flow velocity and depth, as well as bed slope and friction, also affect the process [*Bartsch-Winkler and Lynch*, 1988; *Chanson*, 2011a; *Shi et al.*, 2014].

Tidal bores play a significant role on the ecology, morphodynamics, and sedimentary structures of an estuary [*Chen et al.*, 1990; *Donnelly and Chanson*, 2005; *Greb and Archer*, 2007; *Fan et al.*, 2012, 2014; *Fielding and Joeckel*, 2015; *Martinius and Gowland*, 2011; *Reungoat et al.*, 2017; *Tessier et al.*, 2017], as well as on the social activities that take place in this environment. Turbulent mixing and dispersion are enhanced at the passage of a tidal bore [*Koch and Chanson*, 2009; *Pan and Huang*, 2010; *Reungoat et al.*, 2015; *Simpson et al.*, 2004; *Tu and Fan*, 2017], and significant bed erosion and sediment resuspension take place [*Keevil et al.*, 2015; *Khezri and Chanson*, 2012a; *Wang and Pan*, 2018]; the bed material is then aerated being suspended and advected upstream with the bore, and redeposited on the tide's retreat [*Chanson et al.*, 2011; *Furgerot et al.*, 2016; *Lubin et al.*, 2010; *Reungoat et al.*, 2014]. This process has a positive and significant influence on the breeding of many small, estuarine invertebrates such as shrimps, mollusks and worms, which in turn feed several species of fish and provide important feeding grounds for wading birds and estuarine wildlife [for example, *Chanson*, 2011b]. Tidal bores are also a major tourist attraction and provide opportunity for recreational activities such as surfing.

Given their importance and appeal, tidal bores have long been studied theoretically, numerically and experimentally with laboratory and field investigations. However, despite the many studies, and possibly because of the many factors which contribute to determining whether a bore forms or not, the prediction of their occurrence remains a challenge [*Hoitink and Jay*, 2016].

According to *Chanson* [2011a], a tidal bore occurs when tidal range exceeds 4-6 m and the flood tide is confined within a narrow, funnel shaped estuary. However, in addition

to being rather qualitative, field observations do not always support this criterion. Tidal bores are observed, for example, in the Indus River [*Bartsch-Winkler and Lynch*, 1988] with a spring tidal range of just approximately 2.0 m [*Eisma et al.*, 1988] whereas, in the Mezen River, no bore is observed despite the large tidal range of 7.8 m [*Dolgopolova*, 2013].

Based on a scaling analysis of the one-dimensional shallow water equations, *Bonneton et al.* [2016] showed that the occurrence of tidal bore is controlled by two dimensionless parameters, namely the nonlinearity and the friction parameter. Using the data of 21 estuaries, among which 8 are characterized by the presence of tidal bores, they showed that tidal bores occur when the nonlinearity parameter is greater than a critical value, which is an increasing function of the friction parameter; in the space of these two parameters, a curve separating the region in which conditions are such that a bore can form from the region where bores cannot occur has been drawn by eye (details about this criterion are shortly given in the text). However, this criterion lacks a theoretical basis; the problem of setting down a theoretical model, or just a physically based, conceptual model to predict the occurrence of tidal bore is still open. This is possibly because the occurrence of tidal bore is governed by so many factors, as listed above, and none of them prevails over others.

Therefore, there is a clear need of basic studies that look at the kernel of the phenomenon at hand by starting from very simple and schematic geometry and flow conditions, and gradually building up an understanding of why and how a tidal bore occurs and develops, by accounting for an increasing number of factors affecting tidal bore formation. This need has motivated the present work.

In this paper, we approach the problem from a phenomenological point of view. We numerically simulate the tidal propagation in a schematic channel and search for all behaviors that are possibly distinctive of conditions for which either a bore is observed to form or no bores occur. In order to reduce the degrees of freedom of the problem, the framework within which we study the formation and development of a tidal bore is extremely simple. In particular, we consider a rectangular channel of constant width, in uniform subcritical flow, in which the downstream water level is raised at a constant rate. Accordingly, this basic study is just a first step toward a better understanding of the mechanisms promoting the tidal bore formation, and not a concluding work.

Section 2 introduces the methods and shortly describes the numerical model used in the investigation. The results of the numerical simulations are discussed in Sect. 3; more precisely, Sect. 3.1 gives the criterion adopted to identify, from the results, if the free surface wave produced by the rising of the downstream level has evolved toward a well formed bore or not; in Sect. 3.2, some criteria to predict the occurrence of a tidal bore, on the basis of external parameters, are proposed and discussed; in Sect. 4, the best performing criterion is then extended to predict tidal bore occurrence in real estuaries, and the predictions of the criterion are compared with the available field data. Conclusions are summarized in Sect. 5.

2 Materials and methods

2.1 The idealized framework adopted in the study

Among the many mechanisms and conditions that affect the process of tidal bore formation, the more relevant are *i*) the rate of tidal level rise [for example, *Chanson*, 2011b; *Bonneton et al.*, 2016], *ii*) the characteristics of the incoming flow, typically flow depth and velocity [for example, *Cai et al.*, 2014; *Filippini et al.*, 2018], *iii*) the funneling shape of the estuary that deforms the tidal wave by steepening the rising limb, hence enhancing the rate of level rise [for example, *Friedrichs and Aubrey*, 1994; *Lanzoni and Seminara*, 1998; *Savenije*, 2012; *Toffolon et al.*, 2006], *iv*) the channel bed profile that also affects the
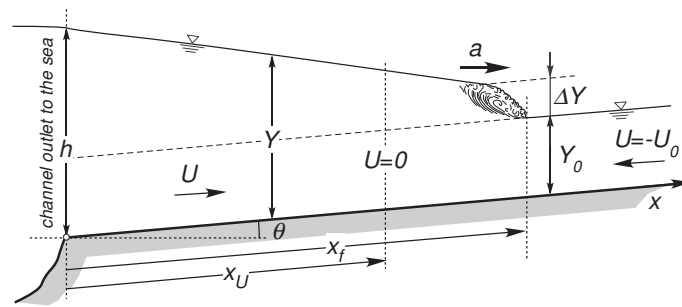
Figure 1. Schematic of the surge propagating upstream against a uniform flow of depth Y_0 and velocity U_0, with notations. ΔY is the bore front height, x_f denotes the position of the foot of the front, that is, the most upstream cross section where undisturbed water level is affected by the propagating tide; x_U denotes the position of the cross section where the flow reverses, that is, the velocity is zero.

characteristics of the propagating tidal wave [for example, *Cai et al.*, 2012; *Savenije et al.*, 2008; *Shi et al.*, 2014], and *v*) the irregular shape of cross-sections, which may introduce additional dissipative processes, alter the wave celerity, and produce reflections and/or distortions of the bore front [for example, *Bonneton et al.*, 2011; *Pan et al.*, 2007; *Shi et al.*, 2014; *Treske*, 1994].

Among these mechanisms and processes, some are necessary for a bore to form (for example, the rise of downstream water level), whereas others just act to promote and enhance the bore formation [for example, the funneling shape, *Filippini et al.*, 2018]. In fact, tidal bores can also form in straight channels (for example, the tidal bore on the River Winster, UK) and are often studied using straight flumes with rectangular or trapezoidal cross-section, constant width and bed slope [*Chanson*, 2009, 2010; *Hayami et al.*, 1955; *Koch and Chanson*, 2008, 2009; *Favre*, 1935; *Prüser and Zielke*, 1994; *Treske*, 1994]. This is the reason that these estuary features are not considered in this first step study.

In order to reduce the degrees of freedom of the problem, the framework within which we study the formation and development of a tidal bore is extremely simple. The present study considers a rectangular channel of constant width, and assumes the bottom slope, s, small enough so that $cos\theta \approx 1$, $sin\theta \approx tan\theta = s$, with θ the angle of the channel bed to the horizontal (Fig. 1). The incoming flow is assumed uniform with water depth Y_0 and bulk velocity U_0. The rate of tidal level rise is assumed constant so that the downstream level, h, is imposed to increase linearly in time from $h = Y_0$ at $t=0$. Although the framework is very simple and schematic, the problem is actually rather involved and its solution is far from being trivial.

In the numerical simulations, the rate of downstream level rise is chosen based on typical semi-diurnal tides. More precisely, we considered the rising rate of level of a sinusoidal tide, averaged over a time interval of about one hour around the instant in which the rise rate is maximum. We find $dh/dt \approx 3T_R\omega_0$, with T_R the tidal range and ω_0 the tidal angular frequency ($\omega_0 = 2\pi/T$, with T the tidal period). For this reason, considering the typical tidal range occurring in real estuaries where tidal bores form, we used a rate of downstream level rise of 1-4 m/h. Since the funneling shape of real estuaries acts to deform the tidal wave thus enhancing the rate of level rise during of the flooding tide [for example, *Bonneton et al.*, 2015; *Friedrichs*, 2010; *Savenije*, 2012], in some cases we also considered a level rise rate of 6 m/h.

In addition, most of simulations last less than 1.0-2.0 hours; only in few cases the simulations are protracted up to 4.0 hours. Conditions used in the numerical investigation are summarized in Table 1.

Table 1. Summary of conditions used in the numerical investigation.

Parameter	Symbol	Unit	Value
bottom slope	s	(-)	$4.4 \cdot 10^{-6} - 5.0 \cdot 10^{-4}$
uniform flow depth	Y_0	(m)	$0.27 - 6.71$
uniform flow velocity	U_0	(m/s)	$0.06 - 0.94$
uniform flow Froude number	F_0	(-)	$0.015 - 0.29$
small wave celerity	c_0	(m/s)	$1.6 - 8.1$
rate of sea level rise	dh/dt^a	(m/h)	$1.0 - 4.0$

[a]Few simulations use a rate of sea level rise of 6 m/h.

2.2 The numerical model

The problem schematized in Fig. 1 is essentially one-dimensional; nonetheless, we use an available and well tested two-dimensional hydrodynamic model [*Defina et al.*, 2008a,b; *Viero et al.*, 2013], also in view of using the same model to simulate the 2D flow in a converging estuary. The Godunov-type, shock-capturing scheme solves the depth-averaged shallow water equations, written in conservative vector form, on unstructured triangular grids based on the finite volume technique. Bottom elevations are defined at the grid nodes and are assumed to vary linearly within each element of the mesh; the second-order accurate description of the channel bed allow to properly deal with sloping channel [*Begnudelli and Sanders*, 2006; *Defina and Viero*, 2010]. In order to avoid the generation of unphysical discontinuities at cell faces even in the case of smooth flows, data at cell faces are reconstructed by selecting either primitive or conservative variables according to the local Froude number, according to the adaptive approach proposed by *Begnudelli et al.* [2008]. First-order adaptive schemes, which utilize a second-order accurate description of bottom elevations, were shown to be robust, efficient, and accurate for many engineering applications [*Begnudelli et al.*, 2008]. Moreover, the Local Time Stepping method proposed by *Sanders* [2008] is used to improve the model performance in terms of computational cost.

Simulations are performed over a rectangular domain having a length in the range 10 km<L<40 km depending on the distance traveled by the surge before vanishing [*Viero et al.*, 2017] or before turning into a quasi-stationary hydraulic jump [*Defina et al.*, 2008c]. Preliminary simulations are carried out by progressively doubling the grid resolution until the maximum relative difference, in terms of both water depth and bore position, was less than 10^{-3}. By this procedure, the typical size of grid elements is found to be 2.5 m in the flow direction; in some cases, the size is reduced to 1.0 m. Since the problem is essentially one-dimensional, the domain width can be arbitrarily chosen. In the simulation, the domain width is set approximately equal to the longitudinal size of grid elements to make their shape as regular as possible, thus increasing model accuracy and performance. The 2D finite volume model, forced into 1D condition as in the present study, has been validated against analytical solutions derived from *Toro* [2000] and *Toro* [2001]; the results are reported as supporting information.

3 Results and discussion

The illustration of the numerical results is split into two parts. In the first part (Sect. 3.1), the results of the simulations are analyzed and the behavior of the swell wave propagating upstream into the channel is studied in order to find a criterion allowing to establish if a bore has actually formed or not. In the second part (Sect. 3.2), we look for, and propose some criteria that allow to predict when a bore forms and develops, based on easily mea-

surable external parameters. In addition, we compare the prediction of the most effective criterion, among those proposed, with the available data from real estuaries.

Most of the results are presented in nondimensional form. Vertical lengths are scaled by the flow depth, Y_0, of the incoming uniform flow, whereas horizontal lengths are scaled by the ratio Y_0/s, (the bottom slope is here introduced to make nondimensional vertical and horizontal lengths comparable, given that in shallow flows horizontal lengths are much greater than vertical lengths). Velocity is scaled by the small wave celerity $c_0 = \sqrt{gY_0}$, where g is gravity, and time is scaled by the ratio between the horizontal length scale and the small wave celerity, $\tau = Y_0/(c_0 s)$ [see *Viero et al.*, 2017]. Nondimensional variables are denoted with an asterisk (for example, nondimensional time is $t^* = t/\tau$, and the nondimensional water depth at the outlet is $h^* = h/Y_0$).

3.1 Analysis of the numerical results

A criterion is needed to identify, from the results of the numerical simulations, if the free surface wave, produced by the rising of the downstream level, has evolved toward a well formed a bore or not.

Based on field measurements by *Bonneton et al.* [2015], *Bonneton et al.* [2016] assume that, in their numerical simulations, a bore has formed when the maximum free surface steepness, in time and in space, goes greater than the threshold value of 0.001. The criterion looks reasonable and it is partly supported by the results of present numerical simulations; however, our study suggests that a suitable threshold value should depend on the Froude number of the incoming flow.

A more physically based criterion, to ascertain from the results of the numerical simulations whether a tidal bore has formed or not, is proposed. To illustrate the criterion, some preliminary discussion of the results of present numerical simulations is needed.

In order to describe the evolution of the perturbed flow field toward the possible formation of a bore, we focus on specific characteristics of the swell propagating upstream in the channel, and identify three characteristic cross sections, *i)* the foot of the front, that is, the most upstream cross section where undisturbed water level is affected by the propagating tide; this cross section moves with a velocity $a_f = dx_f/dt$, x_f being its position; *ii)* the cross section where the steepness of the water surface attains a maximum; this cross section moves with a velocity $a_s = dx_s/dt$, x_s being its position; in addition, the maximum free surface steepness is denoted with $S(t) = \max\{-dh/dx\}$ and its maximum value in time is denoted with S_{max}; and *iii)* the cross section where the flow reverses, that is, where the bulk flow velocity is zero; this cross section moves with a velocity $a_U = dx_U/dt$, x_U being its position (see Fig. 1).

Importantly, numerical simulations show that, in the presence of a developing or a well formed bore, the following constraint holds

$$x_U(t) \le x_s(t) \le x_f(t) \tag{1}$$

Accordingly, we can define two positive distances, $\Delta x_{Uf} = x_f - x_U$ and $\Delta x_{Us} = x_s - x_U$, for which the condition $\Delta x_{Uf} \ge \Delta x_{Us}$ holds.

Three different behaviors are observed. The first one is shown in Fig. 2. During the early stage of the process, the tidal levels propagate upstream and the foot of the front has approximately a constant velocity $a_f \approx a_0 = c_0 - U_0$. The flow at the most downstream section (that is, the channel outlet) gradually reduces its velocity while it goes to zero at time t_{U0}^* (see Fig. 2a). From that moment on, the cross section where the flow reverses penetrates the channel at the nearly constant velocity a_U that is greater than a_f so that, from time t_{U0}^* on, the distance Δx_{Uf} reduces (Fig. 2b). At $t^* = t_1^*$ ($t_1^* \approx 0.32$ in Fig. 2a)

the flow in the two sections start interacting; the foot of the front sharply increases its velocity while the cross section where the flow reverses slows down until, at $t^* = t_2^*$ ($t_2^* \approx$ 0.4 in Fig. 2a), both sections start moving with approximately the same velocity and the distance Δx_{Uf}, becomes negligibly small (Fig. 2b). From $t^* = t_1^*$ on, the front steepness starts growing fast and it gradually reaches its maximum value ($S_{max} \approx 0.05$ in Fig. 3b). When this behavior occurs we assume that a bore actually forms.
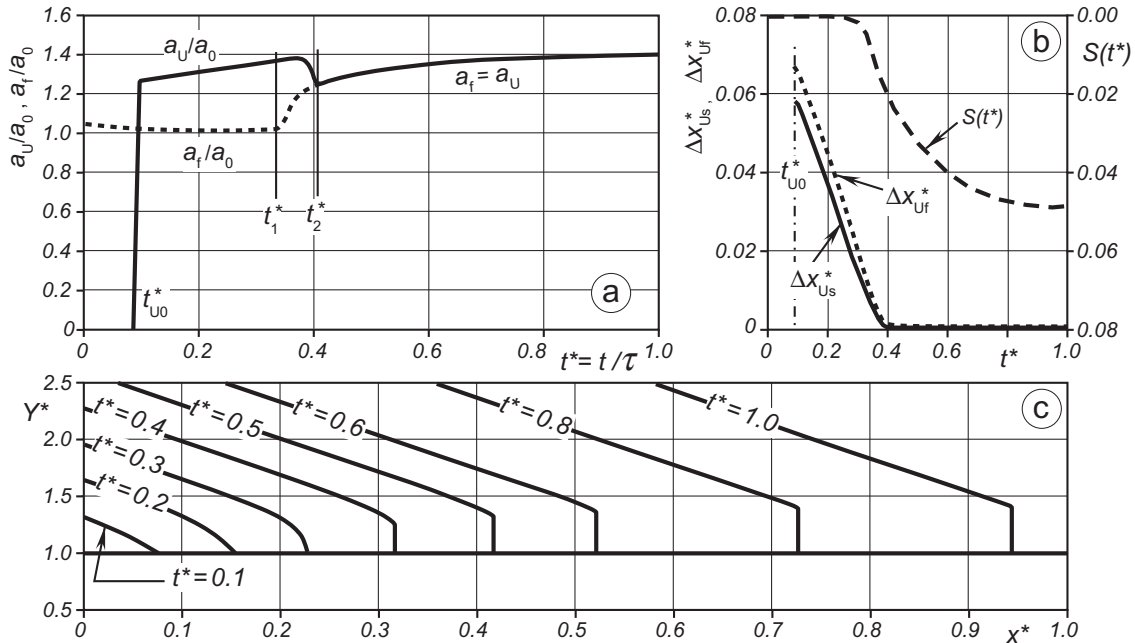

Figure 2. Results of numerical simulation for the case $s=5\cdot10^{-5}$, $F_0=0.23$, $\tau=7085$ s, $dh/dt=2$ m/h; *a*) velocities of cross section where the flow reverses, a_U, and foot of the bore, a_f as they vary with time; *b*) distances Δx_{Uf} and Δx_{Us}, and maximum free surface steepness, $S(t^*)$, as they vary with time; *c*) water surface profiles at different times.

A second, typical behavior is shown in the upper panels of Fig. 3. In this case, when $t^* > t_{U0}^*$, the velocity a_U turns out to be smaller then a_f (Fig. 3a). As a consequence, the distance Δx_{Uf} increases with time, and the cross section where the flow reverses does not approach the foot of the developing bore (Fig. 3b). The maximum free surface slope grows to values smaller than or comparable to the bed slope and then decreases (Fig. 3b). Water surface profiles shown in Fig. 3c confirm that the swell front is weakly sloping while propagating in the channel. In this case, we assume that a bore does not form.

In the third case, an intermediate behavior is observed (lower panels of Fig. 3). In this case the early stage of the process is similar to that shown in Fig. 2, leading to the bore formation. However, from time $t^* = t_2^*$ ($t_2^* \approx 0.5$ in Fig. 3d) the cross section where the flow reverses slows down and its velocity remains below that of the foot of the front. Therefore, from $t^* = t_2^*$ on, both the distances Δx_{Uf} and Δx_{Us} increase (Fig. 3e) pointing out that the front weakens. This is confirmed by the behavior of $S(t)$ shown in Fig. 3e and by the free surface profiles of Fig. 3f. A further interesting occurrence occurs at $t^* \approx 1.28$ (Fig. 3e), when the distance Δx_{Uf} sharply reduces thus implying that the bore front definitely vanished. This is even more evident in Fig. 4 where the free surface steepness, $-dh/dx$, is plotted as a function of the longitudinal position, x^*, at different times.
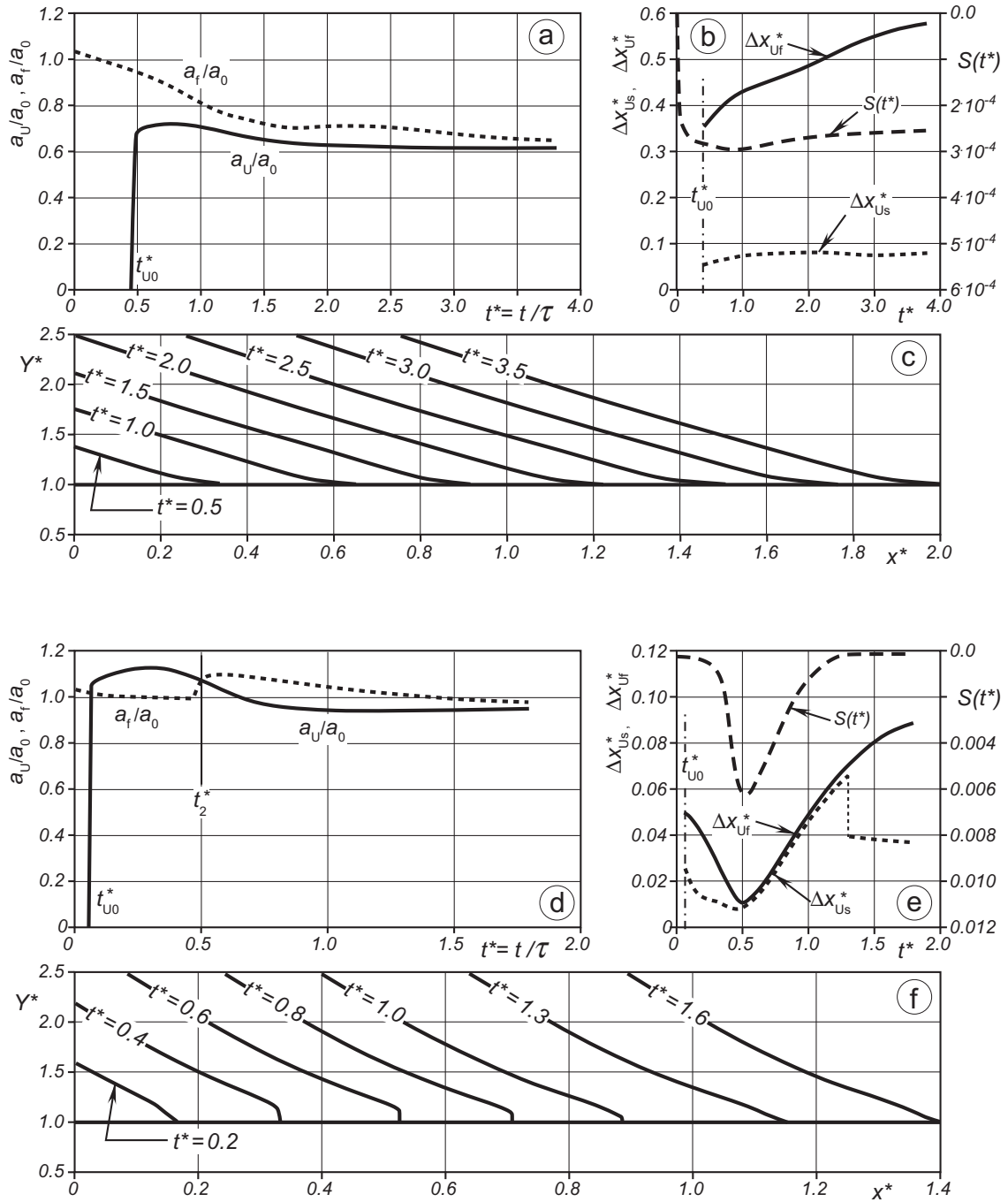
Figure 3. (a–c) Same as in Fig. 2 for the case $s=2\cdot10^{-4}$, $F_0=0.19$, $\tau=1890$ s, $dh/dt=2$ m/h; (d–f) Same as in Fig. 2 for the case $s=6.9\cdot10^{-5}$, $\tau=6060$ s, $F_0=0.14$, $dh/dt=3$ m/h.

In this third case, a bore actually forms but its fate is to rapidly vanish. The front height (Fig. 3f) and steepness (Fig. 4) quickly grows to relatively large values and then decreases until a wavefront cannot be recognized anymore. In this case we state that a weak bore forms.

Overall, the results of the numerical simulations suggest that there are three distinctive behaviors typical of conditions in which a bore or weak bore occurs, or no bore forms
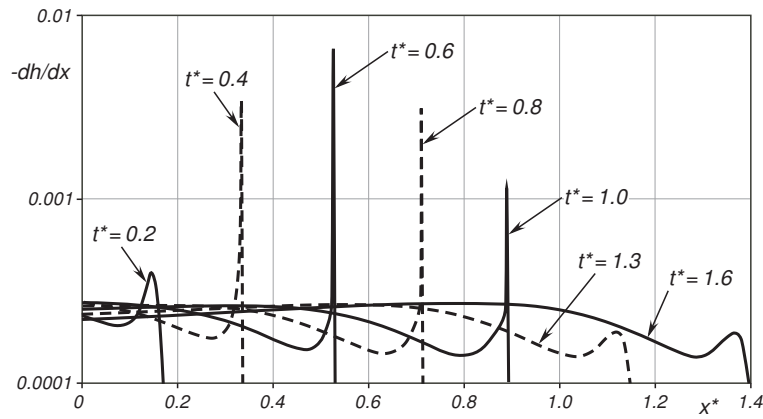
Figure 4. free surface steepness, $-dh/dx$, along the free surface profiles at different times for the case s=6.9·10^{-5}, τ=6060 s, F_0=0.14, dh/dt=3 m/h. (see lower panels of Fig. 3).

at all. In the following, bore occurrence is identified from the results of the numerical simulations according to these behaviors.
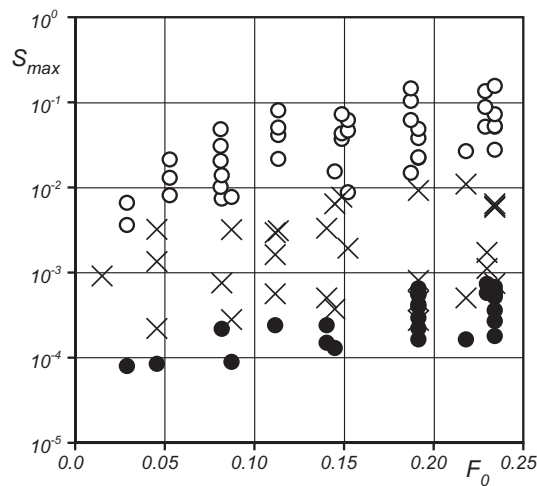

Figure 5. Maximum value of the free surface steepness, S_{max}, as a function of the Froude number of the incoming flow. White and black circles denote conditions in which bores form and do not form, respectively; crosses denote conditions in which weak bores form.

Figure 5 shows the maximum value of the free surface steepness, S_{max}, as a function of the Froude number of the incoming flow and it actually compares the proposed criterion to identify, from the results of the numerical simulations, if a bore forms or not, with that proposed by *Bonneton et al.* [2015]; open and full symbols denote conditions in which a bore forms and it does not form, respectively; crosses denote conditions in which a weak bore forms. When S_{max} is greater than 0.1%, bores actually form, although some of them are weak bores. However, the behavior of points plotted in Fig. 5 suggests that the threshold steepness for bore formation should depend on F_0 and, in particular, it should increase with F_0 increasing [*Chanson*, 2009].

3.2 Possible criteria to predict the occurrence of tidal bore

Based on deductive reasoning and with reference to the schematic flow configuration of Fig. 1, different possible criteria are proposed in order to predict the occurrence of tidal bore as a function of suitable external parameters. Each criterion is then checked against the results of numerical simulations. To this aim, the probability of success is computed as the ratio of the number of times the prediction of the criterion is correct to the total number of numerical simulations. However, given the relatively small number of simulated conditions, the chance of success alone is not considered effective enough. Therefore, when the criterion fails, we also check if conditions are close to the threshold boundary; if not, the criterion is rejected even if the chance of success is relatively large.

Criterion #1. We preliminarily show that the rate of tidal level rise alone does not allow to predict if a bore can form. This is apparent in Fig. 6 where dh/dt is plotted against the Froude number F_0.

On average, the probability of occurrence of conditions conducive to bore formation increases with dh/dt increasing. However, the distribution of points plotted in Fig. 6 does not show any particular trend.
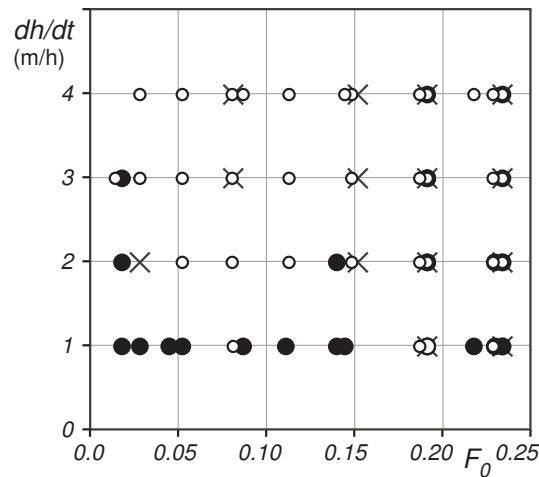

Figure 6. Rate of downstream level rise as a function of the Froude number of the incoming flow. Symbols are the same as in Fig. 5.

Criterion #2. From the analysis of the numerical results it emerges that, for either a weak or strong bore to form, the velocity a_{U0} must be greater than a_f. As a first approximation, when $t \approx t_{U0}$, we can assume that $a_f \approx a_0$ so that the criterion for bore formation reads

$$a_{U0}^* \geq a_0^* \qquad (2)$$

in which the velocities a_{U0} and a_0 are scaled with c_0.

Figure 7 shows that this criterion has a good prediction capacity. If the cases in which a weak bore forms are excluded, the criterion has a 98.6% success rate. The main drawback of this criterion stems from the difficulty of predicting a_{U0}.

Criterion #3. Close inspection of the computed free surface profiles, and as they evolve with time, highlighted the relative importance of the growth rate of downstream level, which, to some extent, controls the flow rate, and hence the water volumes, enter-
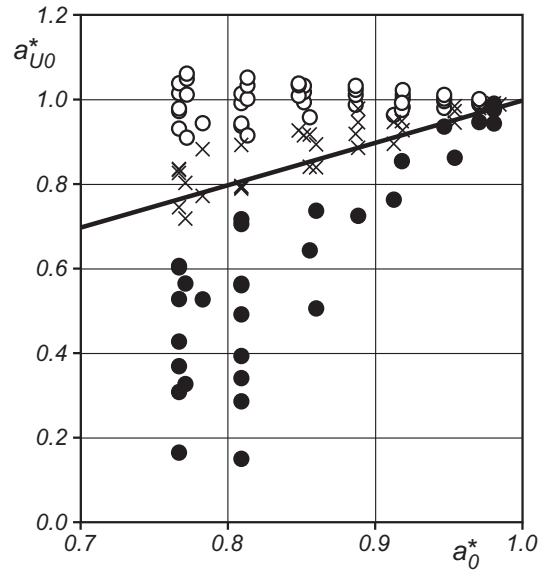
Figure 7. Non dimensional velocity a_{U0}^* as a function of a_0^*; symbols are the same as in Fig. 5. Also plotted is the line $a_{U0}^* = a_0^*$.

ing the channel from the sea, with respect to the speed of the wavefront, which, if large, promote the spreading of these volumes over a longer channel reach. If dh^*/dt^* is large compared to a_f^*, the water from the sea is compressed within a short space and it acts to push the front upstream in order to find more room, this way promoting the formation of a bore. On the contrary, if dh^*/dt^* is small compared to a_f^*, the small volumes of water from the sea are spread over a longer channel reach so that the free surface elevation gently reduces from the sea to the foot of the wavefront and the bore does not form.

As above, during the early stage of the process, $a_f \approx a_0$ can be reasonably assumed; accordingly, the ratio $(dh^*/dt^*)/a_0^*$ could profitably be used to distinguish whether a bore forms or not. According to this criterion, a bore forms if

$$\frac{dh^*}{dt^*} \geq \alpha_1 \, a_0^* \qquad (3)$$

with α_1 a suitable threshold value.

A satisfactory result is obtained for $\alpha_1 = 2.8$ (see Fig. 8). If the cases in which a weak bore develops are excluded, the criterion has a success rate of 91.5 %. However, it can be observed that the line $dh^*/dt^* = 2.8\,a_0^*$ separating conditions for the formation and nonformation of a bore does not follow, qualitatively, the way in which the plotted points actually distribute; more precisely, it seems that the threshold value should grow with growing a_0^*. Moreover, when a_0^* is greater than approximately 0.95, that is, when F_0 is smaller than 0.05, the criterion actually fails. For these reasons, this criterion is unsatisfactory, and it is rejected.

Criterion #4. The results of the numerical simulations highlight the presence of two competing processes. The first, just described above, is controlled by the ratio $(dh^*/dt^*)/a_0^*$; the second stems from the observation that, when the incoming flow is subcritical, the fate of a positive surge is to gradually reduce its height and velocity until vanishing [*Viero et al.*, 2017].
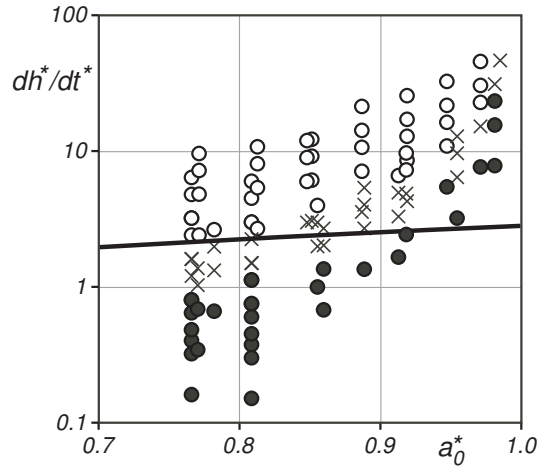
Figure 8. The results of numerical simulations plotted on the $(a_0^*, dh^*/dt^*)$ diagram; symbols are the same as in Fig. 5. The solid curve is the line $dh^*/dt^* = 2.8\, a_0^*$.

For a problem similar to the present one, that is, for the case of a positive surge generated in a sloping channel by the instantaneous closure of a downstream gate, *Viero et al.* [2017] showed that the distance, L_M, traveled by the surge before vanishing is

$$L_M^* = L_M \frac{s}{Y_0} = \frac{2F_0}{1 - F_0^2} \tag{4}$$

The process studied by *Viero et al.* [2017] is a bit different from the present one since in their case the flow never reverses; nonetheless, we speculate that the ratio $1/L_M^*$ can be used to measure the intensity of the mechanisms that act against the bore formation or to weaken the bore once formed.

Accordingly, the ratio between $(dh^*/dt^*)/a_0^*$ and $1/L_M^*$ should measure the propensity for a bore to form; we then assume that a bore forms when this ratio is greater than a threshold value, α_2

$$\frac{L_M^*}{a_0^*} \frac{dh^*}{dt^*} \geq \alpha_2 \tag{5}$$

With Eq. (4), the above condition is rearranged to read

$$\frac{dh^*}{dt^*} \geq \alpha_2 \frac{(1 - F_0)(1 - F_0^2)}{2F_0} \tag{6}$$

With $\alpha_2 = 1$, this condition is found to hold rather well (see Fig. 9). If the cases in which a weak bore forms are excluded, the criterion has a 100% success rate. In addition, the curve separating the region where conditions are such that a bore is predicted to form, from the region where no bore can establish, has a behavior that qualitatively follows the way in which the plotted points distribute.

The two dashed lines of Fig. 9 are obtained from Eq. (6) with $\alpha_2 = 1.2$ (upper curve) and $\alpha_2 = 0.65$ (lower curve), and they enclose a region on the $(F_0, dh^*/dt^*)$ diagram that contains most of conditions for a weak bore to form. This occurrence strengthens the proposed criterion.
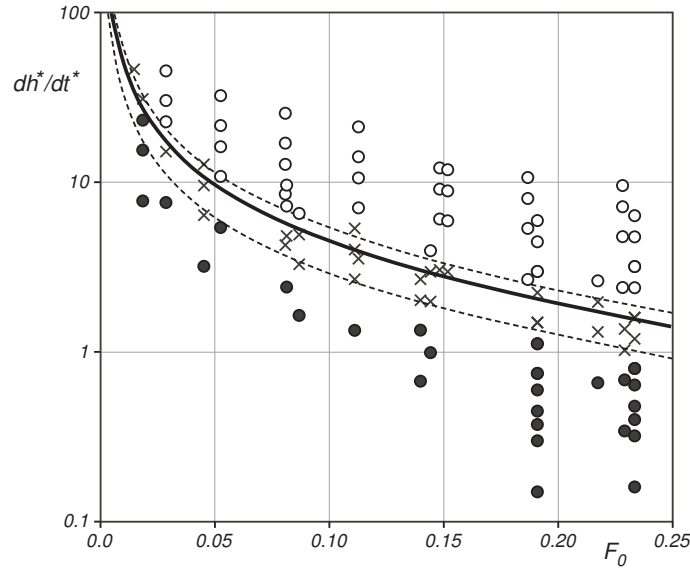
Figure 9. dh^*/dt^* as a function of the Froude number of the incoming flow; symbols are the same as in Fig. 5. The solid curve is given by Eq. (6) with $\alpha_2=1$; the two dashed lines are given by Eq. (6) with $\alpha_2=1.2$ (upper curve), and $\alpha_2=0.65$ (lower curve).

3.3 The height of the bore front

In the frame reference moving with the bore and when neglecting the front acceleration and the local inertia, the continuity and momentum equation across the wavefront allow to estimate the front height and celerity as a function of the Froude number of the incoming flow and of the ratio U_D/U_0, with U_D the flow velocity at the head of the front, positive upstream [*Chanson*, 2004; *Henderson*, 1966]

$$\frac{a}{\sqrt{gY_0}} = -F_0 + \sqrt{1 + \frac{3}{2}\frac{\Delta Y}{Y_0} + \frac{1}{2}\frac{\Delta Y^2}{Y_0^2}} \tag{7}$$

$$\frac{U_D}{U_0}\left(1 + \frac{\Delta Y}{Y_0}\right) = \frac{a}{U_0}\frac{\Delta Y}{Y_0} - 1 \tag{8}$$

Combining the above equations yields a relationship between the front height and flow velocity at the head of the front; in particular, we note that, for a given F_0, the front height increases with U_D increasing.

From the results of the numerical simulations when a bore or a weak bore forms, the maximum front height is extracted. When the bore is weak, the front steepness is not much greater than the free surface steepness behind the front; therefore, in these cases, the estimated front height is affected by an error that is however smaller than 10%.

With the proposed criterion for predicting bore occurrence, the more conditions are above the threshold for tidal bore formation, the more the bore that forms is strong and high. Therefore, from Eq. (6), the parameter

$$\frac{1}{A}\frac{dh^*}{dt^*} \tag{9}$$

with $A = (1 - F_0)(1 - F_0^2)/2F_0$, is likely to control the tidal bore height. In addition, when the Froude number of the incoming flow is relatively small, the relative bore front

height $\Delta Y/Y_0$ given by Eqs. (7) and (8) nearly linearly increases with F_0 (see the inset of Fig. 10). For these reasons, the computed height of the bore fronts are plotted in the $(dh^*/Adt^*, \Delta Y/F_0 Y_0)$ plane (Fig. 10). Also plotted in Fig. 10 are the limits $dh^*/Adt^* = \alpha_2$ with $\alpha_2 = 0.65$ and $\alpha_2 = 1.2$ that, as a first approximation, enclose the region where weak bores occur.

In addition, three gray stripes are drawn in Fig. 10 that denote the regions containing all possible values for $\Delta Y/(Y_0 F_0)$ when $U_D = 0$, $U_D = U_0$, $U_D = 3U_0$ and F_0 is allowed to vary between zero (lower boundary of each stripe) and 0.5 (upper boundary of each stripe).

Figure 10. Relative bore front height scaled by F_0 as a function of $(1/A)dh^*/dt^*$. Symbols are the same as in Fig. 5. The dashed line is from Eq. (9); the regions where a bore, a weak bore or no bore forms are also indicated. The three gray stripes denote the regions containing all possible values for $\Delta Y/(Y_0 F_0)$ when $U_D = 0$, $U_D = U_0$, $U_D = 3U_0$ and F_0 is allowed to vary between zero (lower boundary of each st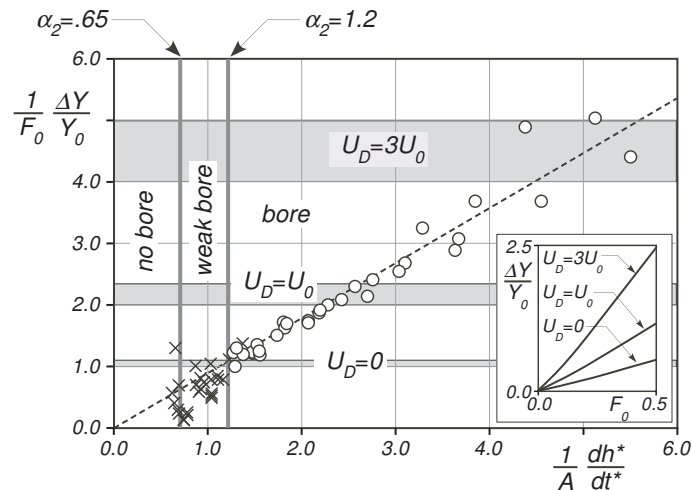ripe) and 0.5 (upper boundary of each stripe). The inset shows the relative front height, $\Delta Y/Y_0$, as a function of F_0, for three values of the relative flow velocity at the front head, U_D/U_0.

It is worth noting that most of weak bores have a relative front height, scaled by F_0, that is smaller than one; hence, the velocity U_D, at the front head, is negative (that is, directed downstream). These conditions are similar to those of a positive surge propagating upstream against a subcritical uniform flow, generated by the instantaneous closure of a downstream gate; in this case, the fate of the surge is to vanish [*Viero et al.*, 2017]. This occurrence actually agrees with present results when a weak bore forms.

On the contrary, strong tidal bores, with a large relative front height, have a positive (that is, directed upstream) velocity at the head; this velocity is also often much greater than U_0. The reversal of bulk flow velocity across the front was found in several field studies [*Chanson et al.*, 2011; *Hoitink and Jay*, 2016; *Pan et al.*, 2007; *Reungoat et al.*, 2014; *Simpson et al.*, 2004; *Wolanski et al.*, 2004; *Xie and Pan*, 2013; *Zhu et al.*, 2012]. Interestingly, the inversion was found to occur almost immediately after the bore passage [*Furgerot et al.*, 2016; *Pan et al.*, 2007], and also significantly after the bore passage [*Reungoat et al.*, 2014], thus confirming that the cross section where the velocity reverses (section "U"in Fig. 1) moves either close to, or significantly behind, the bore, as we found in our numerical simulations.

In the case of a positive surge generated by the rapid closure of a downstream gate in a laboratory flume with uniform flow, the bulk flow velocity downstream the wave-front does not reverse [*Viero et al.*, 2017]. Experimental and numerical analyses showed some transient flow reversal next to the bed and close to the bore passage [*Docherty and Chanson*, 2012; *Khezri and Chanson*, 2012b; *Koch and Chanson*, 2009; *Leng and Chanson*, 2017a,b; *Lubin et al.*, 2010]; however, this occurrence is relatively weak and related to flow separation and recirculation due to the upward deviation of the main flow at the foot of the bore [*Liu et al.*, 2015; *Lubin et al.*, 2010]. In the case of a tidal bore, in which also the bulk flow velocity at the head of the front actually reverses [*Furgerot et al.*, 2016; *Masoud et al.*, 2015; *Simpson et al.*, 2004], the reverse flow is typically much stronger. This is a very important aspect that must be considered in the experimental study of the characteristics of a tidal bore front, in order to properly assess the enhanced mixing and erosion processes related to the flow reversal at the bore passage. Flow reversal was accounted for in few laboratory experiments [*Huang et al.*, 2013; *Rousseaux et al.*, 2016] where, however, the implications of bore passage were not assessed.

It is interesting to observe, in Fig. 10, that points representing the numerical solution arrange, with some scatter, along the dashed line expressed by

$$\frac{1}{F_0}\frac{\Delta Y}{Y_0} = 0.9\frac{1}{A}\frac{dh^*}{dt^*}$$

(10)

4 Application of the present criterion to real estuaries

The schematic framework used in the present study to assess the formation of tidal bore, differs from that of real estuaries mainly because, in the present numerical simulations, the geometry of the channel has not a funnel shape, water levels imposed at the sea do not vary gradually as for a real tide, and the incoming flow is not uniform. However, although important, these aspects may not dramatically affect the conclusions drawn above, at least from a qualitative point of view.

Accordingly, it is interesting to see if the more effective criterion (that is, criterion #4) is (or is far from being) able to predict the occurrence of tidal bores in real estuaries. To this purpose, we rewrite the proposed criterion using the parameters suggested by *Bonneton et al.* [2016], and use the data available in the literature to classify alluvial estuaries in terms of tidal bore occurrence (see Table 2).

Based on a scaling analysis of the one-dimensional shallow water equations, *Bonneton et al.* [2016] showed that the global tidal dynamics is governed by three dimensionless parameters, namely *i*) the dimensionless tidal amplitude

$$\epsilon_0 = A_0/D_0$$

with $A_0 = T_R/2$ the tide amplitude at the estuary mouth, T_R being the tidal range, and D_0 some characteristic water depth; *ii*) the friction parameter

$$\phi_0 = C_{f0}L_{\omega0}/D_0$$

with C_{f0} a characteristic and constant friction coefficient, and $L_{\omega0} = \sqrt{gD_0}/\omega_0$ the frictionless tidal-wave length scale [for example, *Friedrichs*, 2010; *Lanzoni and Seminara*, 1998; *Savenije*, 2012], ω_0 being the tidal angular frequency; *iii*) the convergence ratio

$$\delta_0 = L_{\omega0}/L_{b0}$$

where L_{b0}, which is referred to as the convergence length, is given by $L_{b0} = -B/(dB/dx)$, with B the channel width. *Bonneton et al.* [2016] observed that bore formation is weakly

affected by the convergence ratio δ_0; they speculate that this is possibly because most of real estuaries all have approximately the same δ_0 When plotting the available data in the (ϕ_0, ϵ_0) plane, *Bonneton et al.* [2016] found that a curve can be drawn that definitely separates a region in which conditions are such that tidal bores occur from a region where they do not occur.

Table 2. Flow, tidal and geometric properties of real estuaries.

#	Estuary	tidal bore	T_R (m)	D_0 (m)	U_0 (m/s)	F_0	L_{b0} (km)	c_{f0}	T (h)	ϵ_0	ϕ_0	ΔY (m)	References
1	Chao Phya	no	2.4	7.2	0.54[a]	0.06	109.0	.0039	24.0	0.167	63.0	–	[b]
2	Columbia	no	2.0	10.0	1.0	0.10	25.0	.0031	12.4	0.100	21.7	–	[c]
3	Conwy	no	4.8	3.0	0.5	0.09	6.3	.0051	12.5	0.800	66.1	–	[c]
4	Corantijin	no	2.0	6.5	0.64[a]	0.08	48.0	.0032	12.3	0.154	28.2	–	[b]
5	Daly	yes	6.0	10.0	0.97[a]	0.10	27.0	.0025	12.0	0.300	17.0	1.5	[d,e]
6	Delaware	no	1.3	5.8	0.6	0.08	40.0	.0021	12.5	0.110	19.6	–	[c]
7	Elbe	no	4.0	10.0	1.0	0.10	42.0	.0025	12.4	0.200	17.6	–	[c]
8	Fly	yes	5.1	15.0	0.8	0.07	*n/a*	.0036	12.0	0.169	8.2	2.0	[d,f]
9	Gironde	yes	4.6	10.0	1.0	0.10	44.0	.0031	12.4	0.230	21.7	1.5	[c,g]
10	Hooghly	yes	4.2	5.9	1.0[a]	0.13	25.5	.0015	12.0	0.356	13.3	1.5	[c,d,g,h,i]
11	Trent	yes	6.4	12.0	0.85[a]	0.08	25.0	.0030	12.0	0.267	18.6	1.5	[d,h]
12	Limpopo	no	1.1	7.0	0.36[a]	0.04	50.0	.0032	12.0	0.079	27.1	–	[b]
13	Mae Klong	no	2.0	5.2	0.7[a]	0.10	155.0	.0035	12.3	0.192	33.9	–	[b]
14	Maputo	no	2.8	3.6	0.65[a]	0.11	16.0	.0027	12.3	0.389	31.8	–	[b]
15	Ord	yes	5.0	4.0	2.0	0.32	15.2	.0025	12.0	0.625	26.9	1.2	[c,j]
16	Pungue	yes	6.3	3.5	1.24[a]	0.21	21.0	.0039	12.3	0.900	46.7	0.7	[b,k]
17	Qiantang	yes	6.5	10.0	2.0	0.20	40.0	.0015	12.0	0.325	10.2	3.0	[d,g,h]
18	Scheldt	no	4.0	10.5	0.64[a]	0.06	28.0	.0032	12.3	0.190	22.2	–	[b]
19	Severn	yes	6.0	15.0	1.5	0.12	41.0	.0025	12.4	0.200	14.4	1.5	[c,d,g]
20	Tha Chin	no	2.0	5.3	0.45[a]	0.06	87.0	.0048	24.0	0.189	90.6	–	[b]
21	Thames	no	4.0	8.5	0.6	0.07	25.0	.0050	12.3	0.235	38.1	–	[c]

Symbols are defined in the text. The chosen estuaries are those reported by *Bonneton et al.* [2016]; also included are the data of the Fly River estuary. T_R is the tidal range, D_0, U_0, F_0, and C_{f0} are the characteristic water depth, velocity, Froude number, and friction coefficient, respectively, L_{b0} is the convergence length, T is the tidal period, ϵ_0 is the dimensionless tidal amplitude, ϕ_0 is the friction parameter, and ΔY is the bore height. [a]Estimated according to Eq. (28) in *Toffolon et al.* [2006]; [b]*Savenije* [2012]; [c]*Lanzoni and Seminara* [1998]; [d]*Bartsch-Winkler and Lynch* [1988]; [e]*Bonneton et al.* [2016]; [f]*Canestrelli et al.* [2010] and *Canestrelli et al.* [2014]; [g]*Dolgopolova* [2013]; [h]*Bonneton et al.* [2015]; [i]*Shri and Chugh* [1961]; [j]*Kawanisi et al.* [2017]; [k]*Chanson* [2011a].

Bonneton et al. [2016] performed a large number of numerical simulations to study the propagation of a semidiurnal, sinusoidal tide in a schematic convergent channel of constant depth and exponentially decreasing width. The zero-flux condition is imposed at the inland end of the channel. Using the results of these simulations they could draw isocontour lines of S_{max} in the (ϕ_0, ϵ_0) plane. Interestingly, the shape of these isocontour lines, when S_{max} is in the range 0.0005-0.001, is very similar to the curve *Bonneton et al.* [2016] drew by eye, separating a region in which conditions are such that tidal bores occur from a region where they do not occur. However, as previously observed (see Fig. 5), the use of a threshold value for S_{max} does not allow establishing if a bore has actually formed or not.

In order to compare the prediction of our criterion with the available data for real estuaries, we rewrite condition (6) using the parameters suggested by *Bonneton et al.* [2015], that is, ϕ_0 and ϵ_0.

When the incoming flow is uniform, the friction factor is proportional to the ratio s/F_0^2, so that we can write

$$\phi_0 = \frac{C_{f0}L_{\omega 0}}{D_0} \propto \frac{sL_{\omega 0}}{F_0^2 D_0} = \frac{s\sqrt{gD_0}}{\omega_0 F_0^2 D_0} = \frac{sc_0}{\omega_0 F_0^2 Y_0} \tag{11}$$

where Y_0 is assumed as the characteristic water depth D_0.

The rate of tidal level rise can be expressed as proportional to the tidal range times the tidal angular frequency, that is

$$\frac{dh}{dt} \propto T_R \omega_0 \tag{12}$$

Therefore, the non dimensional rate of tidal level rise can be written as

$$\frac{dh^*}{dt^*} = \frac{d(h/Y_0)}{d(t/\tau)} = \frac{1}{c_0 s}\frac{dh}{dt} \propto \frac{T_R \omega_0}{c_0 s} = \frac{2Y_0 \omega_0}{c_0 s}\epsilon_0 \tag{13}$$

The above equation, with Eq. (11), can be rearranged to read

$$\frac{dh^*}{dt^*} = k\frac{2\epsilon_0}{\phi_0 F_0^2} \tag{14}$$

where k is a calibration factor.

The criterion expressed by condition (6), with dh^*/dt^* given by Eq. (14), reads

$$k\frac{2\epsilon_0}{\phi_0 F_0^2} \geq \alpha_2 \frac{(1-F_0)(1-F_0^2)}{2F_0} \tag{15}$$

that is rewritten as

$$\frac{\epsilon_0}{\phi_0} \geq \alpha_2 \frac{(1-F_0)(1-F_0^2)}{4k} F_0 \tag{16}$$

Figure 11a shows where points denoting conditions when a bore forms (open symbols) and does not form (full symbols) locate in the $(F_0, \epsilon_0/\phi_0)$ diagram. The thick plotted curve is given by Eq. (16) when k=2.1 and α_2=1. Also plotted in Fig. 11a are the curves determined by assuming α_2=1.2 (upper dashed curve) and α_2=0.65 (lower dashed curve).

The available experimental data do not distinguish strong from weak bores; however, it is interesting to observe that points pertaining to estuaries where very strong bores are observed, locate well above the plotted curves.

Finally, we also verify if Eq. 10, suitably rearranged, can predict with some accuracy the front height of bores occurring in real estuaries using the few available data listed in Table 2. It is worth pointing out that, for some of the listed estuaries, more than one value of the bore front height is reported in the literature. For the Qiantang estuary, ΔY=1 − 3 m is given in *Bartsch-Winkler and Lynch* [1988] and ΔY=4 m is reported in *Dolgopolova* [2013], we use the value ΔY=3 m that is in between the two; for the Hoogly estuary, ΔY=2 m is given in *Bartsch-Winkler and Lynch* [1988] whereas *Dolgopolova*
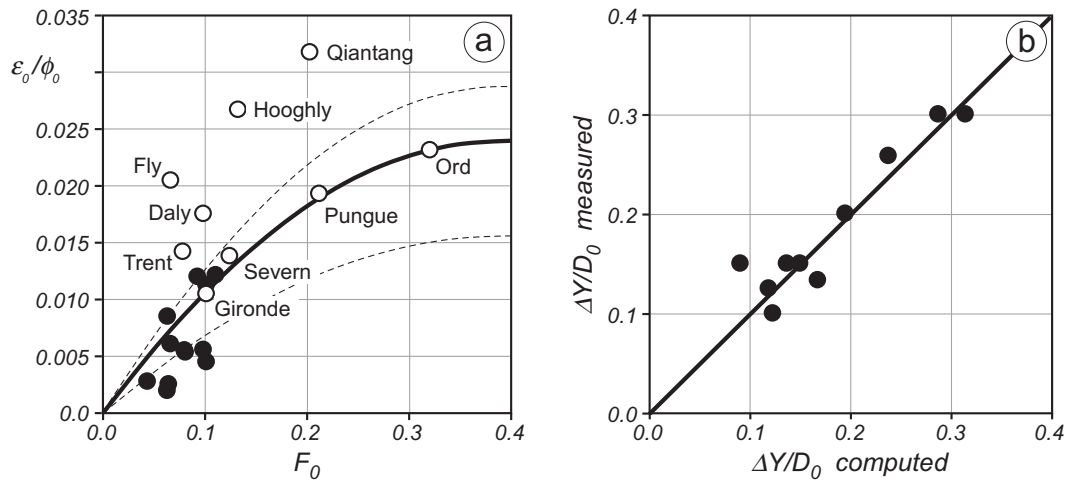
Figure 11. a) Data of real estuaries (as reported in Table 2) where bores do form (white circles) and do not form (black circles) are plotted in the $(F_0, \epsilon_0/\phi_0)$ diagram. The solid curve is given by Eq. (16) with α_2=1; the two dashed lines are given by Eq. (16) with α_2=1.2 (upper curve) and α_2=0.65 (lower curve). b) Comparison between the relative wavefront height, computed with Eq. 17 and k=1.2, and that measured in real estuaries and reported in Table 2. The perfect agreement line is also shown.

[2013] gives the range ΔY=1 − 3 m and *Shri and Chugh* [1961] give the value ΔY=1.5 m, the latter is the value used in the present analysis.

With Eq. (14) for dh^*/dt^*, recalling the expression for A, and replacing Y_0 with D_0, Eq. (10) can be rearranged to read

$$\frac{\Delta Y}{D_0} = \frac{3.6k}{(1 - F_0)(1 - F_0^2)} \frac{\epsilon_0}{\phi_0} \qquad (17)$$

Figure 11b compares the relative bore front height, computed with Eq. (17) and k=1.2, with the available data of real estuaries (see Table 2); the agreement is actually very good.

The relative tidal bore height has been computed with Eq. (10) also for the estuaries where tidal bores do not occur. In this case, $\Delta Y/D_0$ is not negligibly small, however it remains below 0.1.

5 Conclusions

The results of a numerical investigation aimed at improving our knowledge of tidal bore formation are presented and discussed. In order to reduce the problem complexity, this preliminary study used a rectangular channel of constant slope and width, and the bore is generated as the result of rising water levels at the downstream end of the channel, with a constant rate.

Three distinctive behaviors of the swell wave propagating upstream into the channel are observed that are linked to bore, weak bore, or no bore formation. We also found that tidal bore formation is mainly governed by the dimensionless rate of downstream level rise, which must be greater than a threshold value that depends on the Froude number of the incoming flow.

Within the schematic framework used in this study, the analysis of the numerical results, essentially from the phenomenological point of view, has allowed formulating a criterion able to predict the bore formation on the basis of external parameters and, to some extent, able to distinguish weak from strong bores. The criterion has been then rewritten in order to compare its prediction with the available data of real estuaries. This comparison allowed us to recognize that the approach followed in this work can profitably be extended to study the bore formation in the more complex conditions characterizing real estuaries, which include the effects of the typical funnel shape, irregular cross-sections, nonuniform incoming flow, and the gradual variation of tidal sea level.

Although the framework used in the present study is much simpler and schematic than real estuaries, the good agreement between theoretical prediction and real, available data suggests that, in fact, the key features controlling the formation of tidal bores have been likely captured.

References

Bartsch-Winkler, S., and D. K. Lynch (1988), Catalog of worldwide tidal bore occurrences and characteristics, *U.S. Geological Survey Circular*, *1022*, 1–17.

Begnudelli, L., and B. F. Sanders (2006), Unstructured grid finite-volume algorithm for shallow-water flow and scalar transport with wetting and drying, *J. Hydraul. Eng.*, *132*, 371–384, doi:10.1061/(ASCE)0733-9429(2006)132:4(371).

Begnudelli, L., B. F. Sanders, and S. F. Bradford (2008), Adaptive Godunov-based model for flood simulation, *J. Hydraul. Eng.*, *134*, 714–725, doi:10.1061/(ASCE)0733-9429(2008)134:6(714).

Bonneton, P., J. Van de Loock, J.-P. Parisot, N. Bonneton, A. Sottolichio, G. Detandt, B. Castelle, V. Marieu, and N. Pochon (2011), On the occurrence of tidal bores – the Garonne River case, *J. Coast. Res.*, *SI 64*, 1462–1466.

Bonneton, P., N. Bonneton, J.-P. Parisot, and B. Castelle (2015), Tidal bore dynamics in funnel-shaped estuaries, *J. Geophys. Res. Oceans*, *120*, 923–941, doi:10.1002/2014JC010267.

Bonneton, P., A. G. Filippini, L. Arpaia, N. Bonneton, and M. Ricchiuto (2016), Conditions for tidal bore formation in convergent alluvial estuaries, *Estuar. Coast. Shelf Sci.*, *172*, 121–127, doi:10.1016/j.ecss.2016.01.019.

Cai, H., H. H. G. Savenije, and M. Toffolon (2012), A new analytical framework for assessing the effect of sea-level rise and dredging on tidal damping in estuaries, *J. Geophys. Res. Oceans*, *117*, C09,023, doi:10.1029/2012JC008000.

Cai, H., H. H. G. Savenije, and M. Toffolon (2014), Linking the river to the estuary: influence of river discharge on tidal damping, *Hydrol. Earth Syst. Sci.*, *18*(1), 287–304, doi:10.5194/hess-18-287-2014.

Canestrelli, A., S. Fagherazzi, A. Defina, and S. Lanzoni (2010), Tidal hydrodynamics and erosional power in the Fly River delta, Papua New Guinea, *J. Geophys. Res. Earth Surf.*, *115*, F04,033, doi:10.1029/2009JF001355.

Canestrelli, A., S. Lanzoni, and S. Fagherazzi (2014), One-dimensional numerical modeling of the long-term morphodynamic evolution of a tidally-dominated estuary: The Lower Fly River (Papua New Guinea), *Sediment. Geol.*, *301*, 107–119, doi:10.1016/j.sedgeo.2013.06.009.

Chanson, H. (2004), *The Hydraulics of Open Channel Flow: An Introduction*, 2nd edition ed., Elsevier Butterworth-Heinemann, Oxford, UK.

Chanson, H. (2009), Current knowledge in hydraulic jumps and related phenomena. a survey of experimental results., *Eur. J. Mech. B Fluids*, 28, 191–210, doi: 10.1016/j.euromechflu.2008.06.004.

Chanson, H. (2010), Undular tidal bores: Basic theory and free-surface characteristics, *J. Hydraul. Eng.*, 136, 940–944, doi:10.1061/(ASCE)HY.1943-7900.0000264.

Chanson, H. (2011a), *Tidal Bores, Aegir, Eagre, Mascaret, Pororoca – Theory and Observations*, World Scientific Publishing.

Chanson, H. (2011b), Current knowledge in tidal bores and their environmental, ecological and cultural impacts., *Environ. Fluid. Mech.*, 11, 77–98, doi:10.1007/s10652-009-9160-5.

Chanson, H., D. Reungoat, B. Simon, and P. Lubin (2011), High-frequency turbulence and suspended sediment concentration measurements in the Garonne River tidal bore, *Estuar. Coast. Shelf Sci.*, 95, 298–306, doi:10.1016/j.ecss.2011.09.012.

Chen, J., C. Liu, C. Zhang, and H. J. Walker (1990), Geomorphological development and sedimentation in Qiantang Estuary and Hangzhou Bay, *J. Coast. Res.*, 6, 559–572.

Defina, A., and D. P. Viero (2010), Open channel flow through a linear contraction, *Phys. Fluids*, 22, 036,602, doi:10.1063/1.3370334.

Defina, A., F. M. Susin, and D. P. Viero (2008a), Numerical study of the Guderley and Vasilev reflections in steady two-dimensional shallow water flow, *Phys. Fluids*, 20, 097,102, doi:10.1063/1.2972936.

Defina, A., D. P. Viero, and F. M. Susin (2008b), Numerical simulation of the Vasilev reflection, *Shock Waves*, 18, 235–242, doi:10.1007/s00193-008-0159-5.

Defina, A., F. M. Susin, and D. P. Viero (2008c), Bed friction effects on the stability of a stationary hydraulic jump in a rectangular upward sloping channel, *Phys. Fluids*, 20, 036,601, doi:10.1063/1.2841622.

Docherty, J., and H. Chanson (2012), Physical modeling of unsteady turbulence in breaking tidal bores, *J. Hydraul. Eng.*, 138, 412–419.

Dolgopolova, E. N. (2013), The conditions for tidal bore formation and its effect on the transport of saline water at river mouths, *Water Res.*, 40, 16–30, doi: 10.1134/S0097807813010028.

Donnelly, C., and H. Chanson (2005), Environmental impact of undular tidal bores in tropical rivers, *Environ. Fluid. Mech.*, 5, 481–494, doi:10.1007/s10652-005-0711-0.

Eisma, D., P. L. de Boer, G. C. Cadee, K. Dijkema, H. Ridderinkhof, and C. Phillippart (1988), *Intertidal Deposits: River Mouths, Tidal Flats, and Coastal Lagoons*, CRC Press, Boca Raton, Florida.

Fan, D., G. Cai, S. Shang, Y. Wu, Y. Zhang, and L. Gao (2012), Sedimentation processes and sedimentary characteristics of tidal bores along the north bank of the Qiantang Estuary, *Chin. Sci. Bull.*, 57, 1578–1589, doi:10.1007/s11434-012-4993-6.

Fan, D., J. Tu, S. Shang, and G. Cai (2014), Characteristics of tidal-bore deposits and facies associations in the Qiantang Estuary, China, *Mar. Geol.*, 348, 1–14, doi: 10.1016/j.margeo.2013.11.012.

Favre, H. (1935), *Etude théoretique et expérimentale des ondes de translation dans les canaux découverts*, Dunod, Paris, France.

Fielding, C. R., and R. M. Joeckel (2015), Recognition of tidal-bore deposits in the rock record: Towards a facies model, *J. Sediment. Res.*, 85, 118–123, doi:10.2110/jsr.2015.14.

Filippini, A. G., L. Arpaia, P. Bonneton, and M. Ricchiuto (2018), Modeling analysis of tidal bore formation in convergent estuaries, *Eur. J. Mech. B Fluids*, doi: 10.1016/j.euromechflu.2018.01.001.

Friedrichs, C. T. (2010), Barotropic tides in channelized estuaries, in *Contemporary issues in estuarine physics*, edited by A. Valle-Levinson, chap. 3, pp. 27–61, Cambridge University Press, New York.

Friedrichs, C. T., and D. G. Aubrey (1994), Tidal propagation in strongly convergent channels, *J. Geophys. Res.*, *99*(C2), 3321–3336, doi:10.1029/93JC03219.

Furgerot, L., D. Mouaze, B. Tessier, L. Perez, S. Haquin, P. Weill, and A. Crave (2016), Sediment transport induced by tidal bores. An estimation from suspended matter measurements in the Sée River (Mont-Saint-Michel Bay, northwestern France), *C. R. Geosci.*, *348*, 432–441, doi:10.1016/j.crte.2015.09.004.

Greb, S. F., and A. W. Archer (2007), Soft-sediment deformation produced by tides in a meizoseismic area, Turnagain Arm, Alaska, *Geology*, *35*, 435–438, doi: 10.1130/G23209A.1.

Hayami, S., K. Yano, S. Adachi, and H. Kunishi (1955), Experimental studies on meteorological tsunamis traveling up the rivers and canals in Osaka City, Bulletin No. 9, *Tech. rep.*, Disaster Prevention Research Institute, Kyoto University.

Henderson, F. M. (1966), *Open-Channel Flow*, McMillan Publishing Co, New York, USA.

Hoitink, A. F. J., and D. A. Jay (2016), Tidal river dynamics: Implications for deltas, *Rev. Geophys.*, *54*, 240–272, doi:10.1002/2015RG000507.

Huang, J., C. H. Pan, C. P. Kuang, J. Zeng, and G. Chen (2013), Experimental hydrodynamic study of the Qiantang River tidal bore, *Journal of Hydrodynamics*, *25*, 481–490, doi:10.1016/S1001-6058(11)60387-X.

Kawanisi, K., X. Zhu, X. Fan, and I. Nistor (2017), Monitoring tidal bores using acoustic tomography system, *J. Coast. Res.*, *33*, 96–104, doi:10.2112/JCOASTRES-D-15-00172.1.

Keevil, C. E., H. Chanson, and D. Reungoat (2015), Fluid flow and sediment entrainment in the Garonne River bore and tidal bore collision, *Earth Surf. Process. Landforms*, *40*, 1574–1586, doi:10.1002/esp.3735.

Khezri, N., and H. Chanson (2012a), Inception of bed load motion beneath a bore, *Geomorphology*, *153–154*, 39–47, doi:10.1016/j.geomorph.2012.02.006.

Khezri, N., and H. Chanson (2012b), Undular and breaking tidal bores on fixed and movable gravel beds, *J. Hydraul. Res.*, *50*, 353–363, doi:10.1080/00221686.2012.686200.

Koch, C., and H. Chanson (2008), Turbulent mixing beneath an undular bore front, *J. Coast. Res.*, *24*, 999–1007, doi:10.2112/06-0688.1.

Koch, C., and H. Chanson (2009), Turbulence measurements in positive surges and bores, *J. Hydraul. Res.*, *47*, 29–40, doi:110.3826/jhr.2009.2954.

Lanzoni, S., and G. Seminara (1998), On tide propagation in convergent estuaries, *J. Geophys. Res. Oceans*, *103*, 30,793–30,812, doi:10.1029/1998JC900015.

Leng, X., and H. Chanson (2017a), Upstream propagation of surges and bores: Free-surface observations, *Coast. Eng. J.*, *59*, 1750,003, doi:10.1142/S0578563417500036.

Leng, X., and H. Chanson (2017b), Unsteady velocity profiling in bores and positive surges, *Flow Meas. Instrum.*, *54*, 136–145, doi:10.1016/j.flowmeasinst.2017.01.004.

Liu, H., J. Li, S. Shao, and S. K. Tan (2015), SPH modeling of tidal bore scenarios, *Nat. Hazards*, *75*, 1247–1270, doi:10.1007/s11069-014-1374-2.

Lubin, P., H. Chanson, and S. Glockner (2010), Large Eddy Simulation of turbulence generated by a weak breaking tidal bore., *Environ. Fluid. Mech.*, *10*, 587–602, doi: 10.1007/s10652-009-9165-0.

Martinius, A. W., and S. Gowland (2011), Tide-influenced fluvial bedforms and tidal bore deposits (Late Jurassic Lourinhã Formation, Lusitanian Basin, Western Portugal), *Sedimentology*, *58*, 285–324, doi:10.1111/j.1365-3091.2010.01185.x.

Masoud, B. M., K. Kawanisi, and X. H. Zhu (2015), Acoustic investigations of tidal bores in Qiantang River, *J. Jpn. Soc. Civil Eng., Ser. B1 (Hydraul. Eng.)*, *71*, I_139–I_144, doi: 10.2208/jscejhe.71.I_139.

Pan, C., and W. Huang (2010), Numerical modeling of suspended sediment transport affected by tidal bore in Qiantang Estuary, *J. Coast. Res.*, *26*, 1123–1132, doi: 10.2112/JCOASTRES-D-09-00024.1.

Pan, C., B.-Y. Lin, and X.-Z. Mao (2007), Case study: Numerical modeling of the tidal bore on the Qiantang River, China, *J. Hydraul. Eng.*, *133*, 130–138, doi:

10.1061/(ASCE)0733-9429(2007)133:2(130).

Prüser, H.-H., and W. Zielke (1994), Undular bores (Favre Waves) in open channels theory and numerical simulation, *J. Hydraul. Res.*, *32*, 337–354, doi: 10.1080/00221689409498737.

Reungoat, D., H. Chanson, and B. Caplain (2014), Sediment processes and flow reversal in the undular tidal bore of the Garonne River (France), *Environ. Fluid Mech.*, *14*, 591–616, doi:10.1007/s10652-013-9319-y.

Reungoat, D., H. Chanson, and C. E. Keevil (2015), Field measurements of unsteady turbulence in a tidal bore: the Garonne River in October 2013, *J. Hydraul. Res.*, *53*, 291–301, doi:10.1080/00221686.2015.1021717.

Reungoat, D., X. Leng, and H. Chanson (2017), Successive impact of tidal bores on sedimentary processes: Arcins channel, Garonne River, *Estuar. Coast. Shelf Sci.*, *188*, 163–173, doi:10.1016/j.ecss.2017.02.025.

Rousseaux, G., J.-M. Mougenot, L. Chatellier, L. David, and D. Calluaud (2016), A novel method to generate tidal-like bores in the laboratory, *European Journal of Mechanics B/Fluids*, *55*, 31–38, doi:10.1016/j.euromechflu.2015.08.004.

Sanders, B. F. (2008), Integration of a shallow water model with a local time step, *J. Hydraul. Res.*, *46*, 466–475, doi:10.3826/jhr.2008.3243.

Savenije, H. H. G. (2012), *Salinity and Tides in Alluvial Estuaries, 2nd completely revised edition*, salinityandtides.com.

Savenije, H. H. G., M. Toffolon, J. Haas, and E. J. M. Veling (2008), Analytical description of tidal dynamics in convergent estuaries, *J. Geophys. Res. Oceans*, *113*, C10,025, doi:10.1029/2007JC004408.

Shi, J., C. Tong, Y. Yan, and X. Luo (2014), Influence of varying shape and depth on the generation of tidal bores, *Environ. Earth Sci.*, *72*, 2489–2496, doi:10.1007/s12665-014-3156-2.

Shri, R. S., and M. A. Chugh (1961), Tides in Hooghly River, *Int. Assoc. Sci. Hydrol., Bull.*, *6*, 10–26, doi:10.1080/02626666109493212.

Simpson, J. H., N. R. Fisher, and P. Wiles (2004), Reynolds stress and TKE production in an estuary with a tidal bore, *Estuar. Coast. Shelf Sci.*, *60*, 619–627, doi: 10.1016/j.ecss.2004.03.006.

Tessier, B., L. Furgerot, and D. Mouazé (2017), Sedimentary signatures of tidal bores: a brief synthesis, *Geo-Mar. Lett.*, *37*, 325–331, doi:10.1007/s00367-016-0479-x.

Toffolon, M., G. Vignoli, and M. Tubino (2006), Relevant parameters and finite amplitude effects in estuarine hydrodynamics, *J. Geophys. Res. Oceans*, *111*, C10,014, doi: 10.1029/2005JC003104.

Toro, E. F. (2000), *Numerica. A library of source codes for teaching, research and applications*, Numeritek Ltd., Cheshire.

Toro, E. F. (2001), *Shock-capturing methods for free-surface shallow flows*, John Wiley.

Treske, A. (1994), Undular bores (Favre-waves) in open channels – Experimental studies, *J. Hydraul. Res.*, *32*, 355–370, doi:10.1080/00221689409498738.

Tu, J., and D. Fan (2017), Flow and turbulence structure in a hypertidal estuary with the world's biggest tidal bore, *J. Geophys. Res. Oceans*, *122*, 3417–3433, doi: 10.1002/2016JC012120.

Viero, D. P., F. M. Susin, and A. Defina (2013), A note on weak shock wave reflection, *Shock Waves*, *23*, 505–511, doi:10.1007/s00193-013-0452-9.

Viero, D. P., P. Peruzzo, and A. Defina (2017), Positive surge propagation in sloping channels, *Water*, *9*, 518, doi:10.3390/w9070518.

Wang, Q., and C. Pan (2018), Three-dimensional modelling of sediment transport under tidal bores in the Qiantang estuary, China, *J. Hydraul. Res.*, pp. 1–11, doi: 10.1080/00221686.2017.1397781.

Wolanski, E., D. Williams, S. Spagnol, and H. Chanson (2004), Undular tidal bore dynamics in the Daly Estuary, Northern Australia, *Estuar. Coast. Shelf Sci.*, *60*, 629–636, doi:10.1016/j.ecss.2004.03.001.

Xie, D. F., and C. H. Pan (2013), A preliminary study of the turbulence features of the tidal bore in the Qiantang River, China, *Journal of Hydrodynamics*, *25*, 903–911, doi: 10.1016/S1001-6058(13)60439-4.

Zhu, X. H., C. Zhang, Q. Wu, A. Kaneko, X. Fan, and B. Li (2012), Measuring discharge in a river with tidal bores by use of the coastal acoustic tomography system, *Estuar. Coast. Shelf Sci.*, *104–105*, 54–65, doi:10.1016/j.ecss.2012.03.022.